








# Centrosome-mediated microtubule remodeling during axon formation in human iPSC-derived neurons

Feline W Lindhout<sup>1</sup> , Sybren Portegies<sup>1</sup>, Robbelien Kooistra<sup>1</sup> , Lotte J Herstel<sup>1</sup> , Riccardo Stucchi<sup>1,2</sup>, Jessica J A Hummel<sup>1</sup>, Nicky Scheefhals<sup>1</sup> , Eugene A Katrukha<sup>1</sup>, Maarten Altelaar<sup>2</sup> , Harold D MacGillavry<sup>1</sup> , Corette J Wierenga<sup>1</sup> & Casper C Hoogenraad<sup>1,3,\*</sup> 

## Abstract

Axon formation critically relies on local microtubule remodeling and marks the first step in establishing neuronal polarity. However, the function of the microtubule-organizing centrosomes during the onset of axon formation is still under debate. Here, we demonstrate that centrosomes play an essential role in controlling axon formation in human-induced pluripotent stem cell (iPSC)-derived neurons. Depleting centrioles, the core components of centrosomes, in unpolarized human neuronal stem cells results in various axon developmental defects at later stages, including immature action potential firing, mislocalization of axonal microtubule-associated Trim46 proteins, suppressed expression of growth cone proteins, and affected growth cone morphologies. Live-cell imaging of microtubules reveals that centriole loss impairs axonal microtubule reorganization toward the unique parallel plus-end out microtubule bundles during early development. We propose that centrosomes mediate microtubule remodeling during early axon development in human iPSC-derived neurons, thereby laying the foundation for further axon development and function.

**Keywords** axon; centrosome; development; hiPSC-derived neuron; human

**Subject Categories** Cell Adhesion, Polarity & Cytoskeleton; Neuroscience

**DOI** 10.15252/embj.2020106798 | Received 15 September 2020 | Revised 9 February 2021 | Accepted 17 February 2021 | Published online 9 April 2021

**The EMBO Journal (2021) 40: e106798**

## Introduction

Neuronal polarity is established by a series of highly coordinated processes, starting with the formation of the future axon. During axon specification, the first step of axon formation, one of the multiple unpolarized neurites of a neuron displays extensive growth.

Axonal outgrowth critically relies on local cytoskeleton reorganization and growth cone dynamics (Dotti *et al*, 1988; Witte *et al*, 2008). Next, the newly developed axon undergoes significant reorganization as it matures, thereby adopting axon-specific hallmarks required for its function. An essential component of mature axons is the axon initial segment (AIS), a specialized compartment at the base of the axon where specific proteins (e.g., AnkG scaffolds, microtubule-organizing protein Trim46, and voltage-gated sodium and potassium channels) assemble in a highly organized manner (Leterrier, 2018; Freal *et al*, 2019). The AIS is crucial for maintaining neuronal polarity and generating action potentials (APs). The characteristic shaping and subsequent propagation of APs is facilitated by the local clustering of voltage-gated channels at the AIS (Kole *et al*, 2008). Another particularly important aspect of mature axons is their unique microtubule organization. In growing axons, the microtubule network undergoes extensive remodeling, as it shifts from a mixed microtubule polarity to a uniform plus-end out microtubule organization (Yau *et al*, 2016). Trim46 proteins targeted to the AIS act as regulators of these axonal microtubule rearrangements by forming parallel microtubule bundles in proximal axons (van Beuningen *et al*, 2015). In contrast, dendrites contain a microtubule organization of mixed polarities and gain additional minus-end out microtubules during development. This prominent difference in microtubule organization between axons and dendrites is essential for neuronal development and function, as it contributes to polarized cargo transport and the characteristic neuronal morphology (Baas *et al*, 1988; Yau *et al*, 2016). However, while microtubule remodeling in growing axons is important for axon specification and development, the mechanisms driving these microtubule cytoskeletal rearrangements remain largely unresolved.

Centrosomes, the main microtubule-organizing center (MTOC) in most animal cells, are essential for organizing the microtubule network in unpolarized neurons (Tsai & Gleeson, 2005; Stiess *et al*, 2010; Meka *et al*, 2020). These small, membrane-less, and centrally localized organelles are composed of two centrioles surrounded by

1 Cell Biology, Neurobiology and Biophysics, Department of Biology, Faculty of Science, Utrecht University, Utrecht, The Netherlands

2 Biomolecular Mass Spectrometry and Proteomics, Bijvoet Center for Biomolecular Research and Utrecht Institute for Pharmaceutical Sciences, Utrecht University, Utrecht, The Netherlands

3 Department of Neuroscience, Genentech, Inc, South San Francisco, CA, USA

\*Corresponding author. Tel: +31-(0)30-2533894; Fax: +31-(0)30-2513655; E-mail: c.hoogenraad@uu.nl

the pericentriolar material (PCM) (Moritz *et al*, 2000). The majority of the microtubules are typically nucleated from  $\gamma$ -tubulin Ring Complexes ( $\gamma$ TuRCs) embedded in the PCM (Moritz *et al*, 2000). During neuronal development, centrosomes gradually lose their function as MTOC while cilia, the major signaling hubs in polarized cells, are being formed (Stiess *et al*, 2010; Ishikawa & Marshall, 2011). In dissociated rodent neurons, this process was reported to occur during axon development, but the exact temporal relation between axon specification and the declining MTOC function of centrosomes is unclear (Stiess *et al*, 2010). The importance of centrosome function in early neurodevelopment is illustrated by the increasing number of identified mutations in centrosomal proteins causing microcephaly and other neurodevelopmental disorders (Nano & Basto, 2017). However, the precise function of centrosomes as MTOC for different processes of early axon development is still under debate.

Progress in understanding the role of centrosomes during axon specification has been hindered due to a number of technical challenges. In particular, centrosomes are found to display different functions in neurodevelopment in different species, resulting in conflicting findings. This is mostly illustrated by the poor recapitulation of human neurodevelopmental disorders caused by centrosome dysfunction in *Drosophila* and mice, whereas ferrets robustly model these diseases (Basto *et al*, 2006; Castellanos *et al*, 2008; Pulvers *et al*, 2010; Johnson *et al*, 2018). Axon outgrowth can also be differently affected by centrosomes, as this process is perturbed with centrosome dysfunction in mice and peripheral axons of zebrafish, but not in dissociated rodent neurons and central axons of zebrafish (de Anda *et al*, 2010; Stiess *et al*, 2010; Andersen & Halloran, 2012). The molecular mechanisms that underlie the observed species-specific differences remain largely unknown. Another technical challenge is presented by dissociated rodent neurons in culture, which are classically used to study axon developmental processes, as they likely undergo repolarization after being polarized *in vivo* rather than *de novo* polarization (Barnes & Polleux, 2009). Together, this highlights the importance of studying the role of centrosomes in *de novo* polarization using human neurons. The development of human-induced pluripotent stem cells (iPSCs) now enables studying the molecular mechanisms that drive the transition of an unpolarized human neuronal stem cell to a polarized human neuron (Lancaster *et al*, 2013). An additional important feature of human neurons is their significant protracted development, which allows for a more detailed investigation of the temporal processes underlying neuronal polarity (Otani *et al*, 2016; Linaro *et al*, 2019). To illustrate this, neurogenesis occurs after  $\sim 1$  week in rodents, whereas this takes about  $\sim 3$  months in humans, both *in vivo* and *in vitro* (Shi *et al*, 2012; Espuny-Camacho *et al*, 2013; Otani *et al*, 2016; Sousa *et al*, 2017). This profound slower development of human iPSC-derived neurons increases the temporal resolution to study axonal processes, which recently has led to the identification of an additional axon developmental stage in human neurons (Espuny-Camacho *et al*, 2013; Lindhout *et al*, 2020; Otani *et al*, 2016; Linaro, 2019 #9). Altogether, this emphasizes the relevance of studying centrosome functions during axon development in human iPSC-derived neurons as a model system.

In this study, we used a multidisciplinary approach, by combining human iPSC-derived neuron cultures with live-cell imaging, electrophysiology, and mass spectrometry analysis, to examine the

role of centrosomes during early axon development. We found that centrosomes display microtubule-organizing functions during axon specification, similar to non-human neurons, and this function is gradually lost during further axon development. In human neurons specifically, Trim46 localization shifts from a pericentriolar region to the AIS during neuron development, coinciding with the developmental decline of centrosomal microtubule-organizing functions. Differentiation of centriole-depleted neuronal stem cells (NSCs) results in various axonal developmental defects in human neurons, including immature action potential firing, mislocalization of Trim46 proteins, growth cone perturbations, and impaired axonal microtubule remodeling. Together, these data imply that centrosomes mediate microtubule remodeling during axon specification in human iPSC-derived neurons, which is necessary for correct axon formation during further development.

## Results

### Centrosomes display microtubule-organizing functions during axon specification

The centrosome is the primary site for microtubule nucleation and anchoring during early neurodevelopment, and this function gradually declines as neurons mature (Fig 1A) (Stiess *et al*, 2010). To understand the role of centrosomes during early axon development in human neurons, we set out to explore if centrosomes display microtubule-organizing functions during this developmental process in human iPSC-derived neurons. To address this, we tested the microtubule nucleating capacity of centrosomes during development by measuring the endogenous levels of local  $\gamma$ -tubulin, an essential microtubule nucleating protein, at different developmental stages. The neurodevelopmental stages were defined as follows: stage 1 (day 0) as Ki67-positive NSCs; stage 2 (day 7) as differentiated unpolarized MAP2-positive neurons with Trim46-negative processes; stage 3 (day 12) as differentiated polarized MAP2-positive neurons with a Trim46-positive axon (Fig 1B). We identified centrosomes with centriole marker Centrin and quantified the intensity levels of  $\gamma$ -tubulin co-localizing with Centrin (Fig 1B). The  $\gamma$ -tubulin levels at centrosomes were consistently high in stage 1 and stage 2 neurons, and markedly reduced by  $\sim 50\%$  in stage 3 neurons, in line with previous findings in dissociated rat neurons (Fig 1B and C) (Stiess *et al*, 2010). To verify these results, we next performed high-resolution 3D STED imaging to resolve the dense neuronal microtubule network and observed that the microtubule network transformed from a radial organization toward a more non-radial organization during initial neurodevelopment (Fig 1D). This transition marks the decline of microtubule-organizing functions of centrosomes and correlates with the onset of axon development. Together, these results suggest that centrosomes display microtubule-organizing functions during the early developmental stages of human iPSC-derived neurons, which includes the process of axon specification, but not during later stages.

### Centrosome-associated localization of AIS protein Trim46 in early-stage human neurons

An important hallmark of axon development is the assembly of the AIS in the proximal axon, which occurs after the developmental

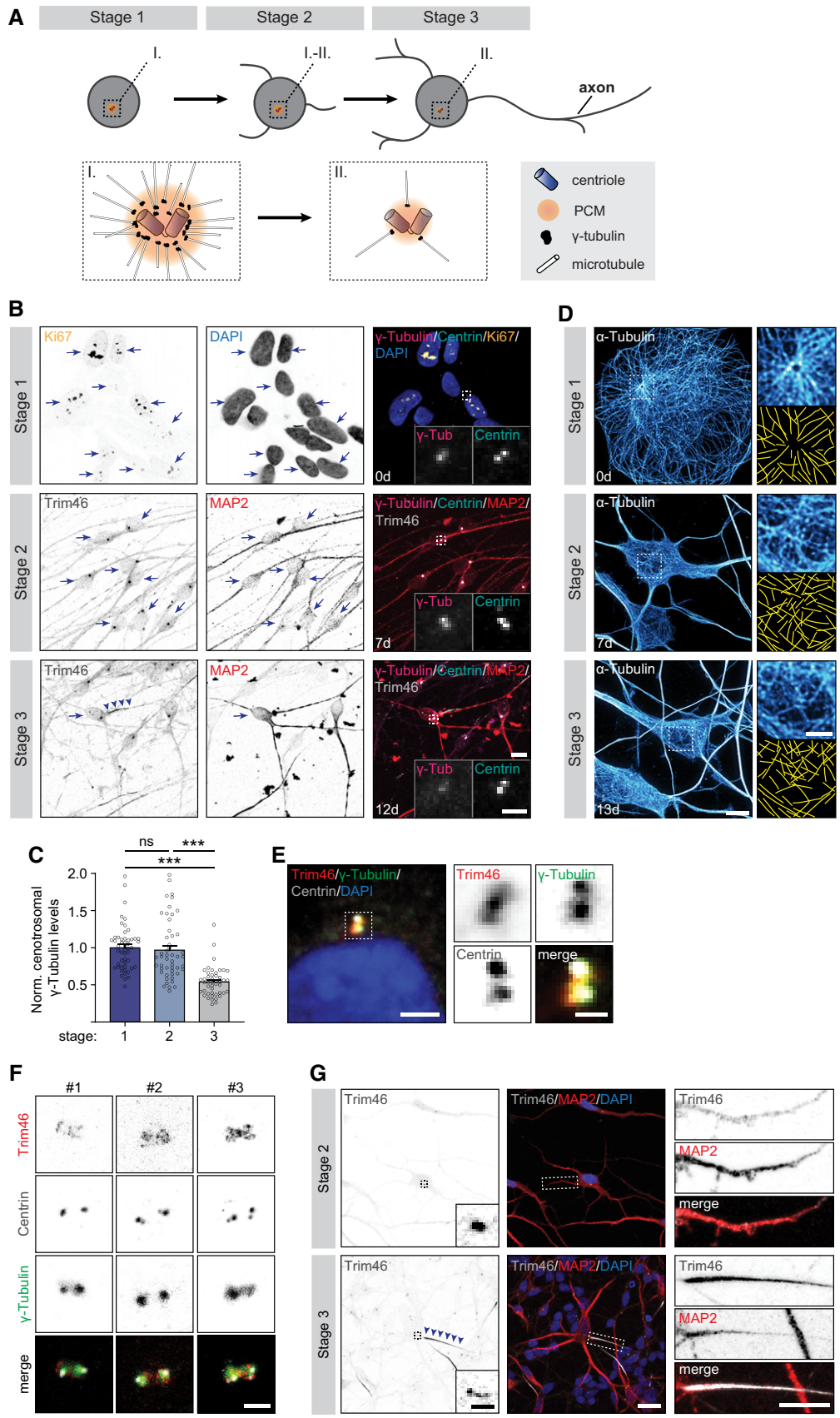


Figure 1.

**Figure 1. Centrosomes display MTOC function and Trim46 appearance during axon specification.**

- A Schematic illustration of centrosomal MTOC function in neurodevelopmental stages 1, 2, and 3 in human iPSC-derived NSCs/neurons.
- B Typical examples of stage 1 (day 0), stage 2 (day 7), and stage 3 (day 12) human iPSC-derived NSCs/neurons immunostained for  $\gamma$ -tubulin and Centrin, marked by arrows. Cells were co-immunostained with Ki67 and DAPI (day 0) or Trim46 and MAP2 (day 7 and 12) to define their neuronal stages. Arrowheads mark the AIS. Scale bar = 10  $\mu$ m in overview, 2  $\mu$ m in zooms.
- C Quantifications of normalized  $\gamma$ -tubulin fluorescent intensities at centrosomes in stage 1, 2, and 3 human iPSC-derived neurons.  $n = 46$ –51 cells in two independent experiments.
- D 3D STED imaging of  $\alpha$ -tubulin in stage 1 (day 0), stage 2 (day 7), and stage 3 (day 13) hiPSC-derived neurons. Scale bar = 5  $\mu$ m in overview, 1  $\mu$ m in zoom.
- E Human iPSC-derived NSCs (day 0) immunostained for Trim46,  $\gamma$ -tubulin, and Centrin. Zoom represents centrosome structure. Scale bar = 5  $\mu$ m in overview, 2  $\mu$ m in zooms.
- F Typical examples of centrosomes of human iPSC-derived NSCs (day 0) with STED imaging of Trim46 and Centrin immunostaining, and confocal imaging of  $\gamma$ -tubulin immunostaining. Scale bar = 1  $\mu$ m.
- G Typical examples of stage 2 and stage 3 human iPSC-derived neurons immunostained for Trim46 and MAP2. Inserts represent centrosomes. Zooms on the right represent a non-polarized neurite or a developing axon in stage 2 or stage 3 neurons, respectively. Scale bar = 20  $\mu$ m in overview, 1  $\mu$ m in insert, 10  $\mu$ m in zoom.
- Data information: Data represent mean  $\pm$  SEM. One-way ANOVA including *post hoc* analysis with Bonferroni correction (C). \*\*\* $P < 0.001$ , ns  $P \geq 0.05$ .

decline of the microtubule-organizing function of centrosomes in dissociated rat hippocampal neurons (Stiess *et al*, 2010). In human neurons, we observed that the AIS protein Trim46 was localized at centrosomes during early neurodevelopment (stage 1–2), as shown by co-localization of Trim46 with the centrosome markers Centrin and  $\gamma$ -tubulin in hiPSC-derived NSCs (Fig 1E). Similarly, centrosome-associated localization of Trim46 was observed in human HeLa cells, but not in dissociated rat hippocampal neurons or mouse IMCD3 cells (Fig EV1A). The human-specific enrichment of Trim46 at centrosomes is confirmed by two additional antibodies, which detected Trim46 at centrosomes in human iPSC-derived neurons but not in primary rat neurons (Fig EV1B). Previous studies showed that Trim46 is a microtubule-binding protein; however, a possible association with centrosomal proteins or structures has not been reported (van Beuningen *et al*, 2015). We sought to identify which centrosome substructure coincided with centrosomal Trim46 structures. Localization experiments by confocal microscopy showed that Trim46 appeared as an oval structure which only partially overlapped with the centriolar and pericentriolar structures marked by Centrin and  $\gamma$ -tubulin, respectively (Fig 1E). To gain more in-depth structural insights, we resolved centrosomal Trim46 structures by STED microscopy and observed that Trim46 appeared as a cloud of punctae surrounding but not overlapping with  $\gamma$ -tubulin structures (Fig 1F). In all cells, we observed a consistent alignment of Trim46 punctae surrounding  $\gamma$ -tubulin, which in turn surrounded Centrin punctae representing the centriolar core. The  $\gamma$ -tubulin structures mark the outer layer of the pericentriolar material as well as the minus-end nucleation sites of microtubules, suggesting that Trim46 localizes near the starting points of centrosomal microtubules (Mennella *et al*, 2012). Together, these data suggest that specifically in human cells, Trim46 localizes to centrosome-associated structures.

#### Trim46 localization shifts from centrosomes to axonal microtubules during development

Studying the localization of Trim46 over time in human neurons revealed a clear decline of Trim46 staining at the pericentriolar region while the intensity of axonal Trim46 levels increased during development. More specifically, the pericentriolar Trim46 levels remained high in stage 2 neurons and were markedly decreased in stage 3 neurons, following the same trend as found

with  $\gamma$ -tubulin (Fig 1G). Consistently, we observed a similar shift of Trim46 staining from centrosomes to dense peripheral microtubules arrays in maturing human iPSC-derived glia cells, which are present at low abundance in the human iPSC-derived neuron cultures (Fig EV1C). Together, these data suggest that Trim46 localization shifts from the pericentriolar region to peripheral axonal microtubule arrays during neurodevelopment.

#### Centrinone-B treatment depletes centrioles in neuronal stem cells

To study the effect of centrosome dysfunction on axon specification, we next aimed to remove centrioles in human iPSC-derived NSCs by using the pharmacological PLK4 inhibitor Centrinone-B. The efficient and robust centriole loss by Centrinone-B treatment has previously been validated in various other cell types (Wong *et al*, 2015). By inhibiting PLK4, Centrinone-B blocks centriole duplication during cell division in proliferating cells, thereby generating a mixed population of cells containing 0, 1, or 2 centrioles. We treated human iPSC-derived NSCs for 0, 2, or 5 days with Centrinone-B prior to neuronal induction and quantified the number of centrioles per cell. Centrioles were defined as puncta with overlapping staining of Pericentrin and Centrin (Fig 2A). We observed successful removal of either 1 or 2 centrioles in ~50% of the NSCs after 2 days of Centrinone-B treatment (Fig 2B). This was not significantly enhanced after a prolonged 5 days of Centrinone-B treatment, likely because cells underwent premature neuronal differentiation and thus terminal cell cycle exit during this time. Centrinone-B treatment increased the number of cells with a characteristic neuron-like morphology, even before inducing neuronal differentiation. This premature neuronal differentiation phenotype is a well-described hallmark of centrosome dysfunction in various *in vivo* or 3D *in vitro* systems, and it underlies microcephaly and other neurodevelopmental disorders (Lancaster *et al*, 2013). We found significantly more neurons upon 2 days of Centrinone-B treatment, measured as the relative number of cells that were positive for neuron differentiation markers MAP2 or  $\beta$ 3-tubulin, or proliferation marker Ki67 (Fig EV2A–E). Together, these data show that Centrinone-B treatment results in successful depletion of centrioles in human iPSC-derived neuronal cells, and that it recapitulates neuronal developmental phenotypes that are broadly associated with centrosome defects.

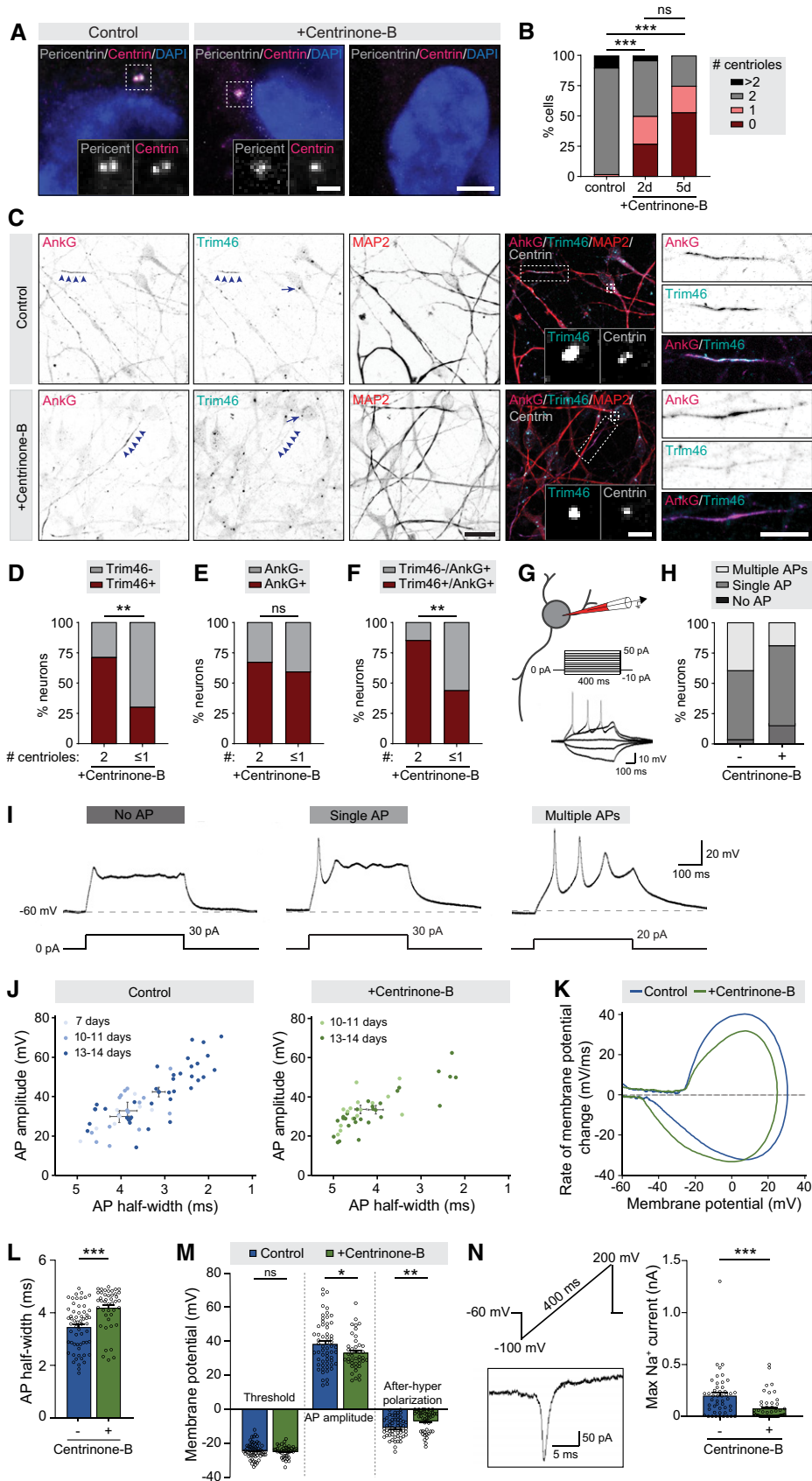


Figure 2.

**Figure 2. Centriole loss in NSCs perturbs subsequent axonal Trim46 targeting and action potential maturation.**

- A Typical examples of Centrinone-B-treated or control human iPSC-derived NSCs immunostained for Pericentrin and Centrin. Inserts represent centriole(s). Scale bar = 5  $\mu\text{m}$  in overview, 2  $\mu\text{m}$  in inserts.
- B Quantifications of the percentage of cells with 0, 1, or 2 centrioles per cell after 0 (control), 2 or 5 days Centrinone-B treatment and prior to neuronal induction.  $n = 48\text{--}51$  cells in two independent experiments.
- C Typical examples of Centrinone-B-treated or control human iPSC-derived neurons (12–15 days) immunostained for AnkG, Trim46, MAP2, and Centrin. Arrowheads mark AIS structures, arrows mark centrosomes. Inserts represent centrosomes, zooms on the right represent AIS structures. Scale bar = 20  $\mu\text{m}$  in overview, 2  $\mu\text{m}$  in insert, 10  $\mu\text{m}$  in zooms.
- D Quantifications of percentage of human iPSC-derived neurons (12–15 days) treated with Centrinone-B containing a Trim46-positive or Trim46-negative process. Neurons are subdivided in populations containing 2 centrioles, or less than 2 centrioles, based on Centrin immunostaining.  $n = 31\text{--}53$  cells in three independent experiments.
- E Quantifications of percentage of human iPSC-derived neurons (12–15 days) treated with Centrinone-B containing an AnkG-positive or AnkG-negative process. Neurons are subdivided in populations containing 2 centrioles, or less than 2 centrioles, based on Centrin immunostaining.  $n = 27\text{--}32$  cells in two independent experiments.
- F Quantifications of percentage human iPSC-derived neurons (12–15 days) treated with Centrinone-B containing AnkG-positive processes that are Trim46-positive or Trim46-negative. Neurons are subdivided in populations containing 2 centrioles, or less than 2 centrioles, based on Centrin immunostaining.  $n = 27$  cells in two independent experiments.
- G *Top*: Schematic illustration of the experimental electrophysiology setup. To determine action potential (AP) frequency, somatic current injections from  $-10$  pA to 50 pA (steps of 5 pA, 400 ms) were applied. *Bottom*: Representative example of evoked AP firing in a Centrinone-B-treated human iPSC-derived neuron, response to hyperpolarizing and first two depolarizing current steps, recorded at day 13.
- H Neuronal excitability was recorded in 54/61 control cells and 53/54 Centrinone-B-treated cells. Percentage of cells firing zero, one or multiple APs in control (4 independent experiments; no AP:  $n = 2$ , single AP:  $n = 32$ , multiple APs:  $n = 22$ ) versus Centrinone-B-treated cultures (3 independent experiments; no AP:  $n = 9$ , single AP:  $n = 34$ , multiple APs:  $n = 10$ ).
- I Representative examples of evoked AP firing in Centrinone-B-treated human iPSC-derived neurons recorded at day 11. Shown is the response to a single depolarizing current step of a neuron that fires no APs, a neuron that fires a single AP and a neuron that fires multiple APs. The offset current ( $I_{\text{hold}}$ ) was adjusted to keep the baseline membrane potential at approximately  $-60$  mV (dashed lines).
- J Scatter plots of AP amplitude versus AP half-width grouped by days after plating for Centrinone-B-treated (10–11 days:  $n = 14$  cells in one independent experiment, 13–14 days:  $n = 28$  cells in three independent experiments) and control (7 days:  $n = 7$  cells, 10–11 days:  $n = 15$  cells in two independent experiments, 13–14 days:  $n = 36$  cells in four independent experiments) human iPSC-derived neurons.
- K Phase plots of a representative AP of a human iPSC-derived neuron treated with Centrinone-B and a control neuron of 13 and 14 days, respectively.
- L AP half-width recorded in Centrinone-B-treated ( $n = 43$  cells in three independent experiments) and control human iPSC-derived neurons ( $n = 59$  cells in four independent experiments).
- M AP threshold, amplitude and after-hyperpolarization recorded in Centrinone-B-treated ( $n = 43$  cells in three independent experiments) and control human iPSC-derived neuron cultures ( $n = 59$  cells in four independent experiments).
- N *Left top*: Schematic representation of the voltage ramp protocol used to determine maximum sodium current; membrane potential was changed from  $-100$  mV to 200 mV in 400 ms. *Left bottom*: Representative example of maximum sodium peak recorded of a control neuron at day 13. *Right*: Maximum sodium peak in Centrinone-B-treated ( $n = 52$  cells in three independent experiments) and control human iPSC-derived neurons ( $n = 48$  cells in three independent experiments).
- Data information: Data represent mean  $\pm$  SEM. Chi-square test including *post hoc* analysis with Bonferroni correction (B, D, E, F); Mann–Whitney test (L, M: after-hyperpolarization, N), Student's *t*-test (M: threshold, AP amplitude). \*\*\* $P < 0.001$ , \*\* $P < 0.01$ , \* $P < 0.05$ , ns  $P \geq 0.05$ .

**Centriole loss perturbs axonal targeting of Trim46**

We next asked whether these centriole-deprived and prematurely differentiated neurons upon Centrinone-B treatment follow normal developmental timing and grow functional axons. To investigate the role of centrosomes during axon specification, we assessed if the development of early-stage axons was affected by centriole loss. An important aspect of early-stage axon development is the specific sorting of axonal proteins, including the AIS protein Trim46. Thus, we tested if the axon-specific localization of Trim46 was affected by Centrinone-B-induced centriole removal. Neurons were immunostained with Centrin and Trim46 to correlate centriole number and the presence of axonal Trim46 for each cell (Fig 2C). We observed a marked  $\sim 50\%$  reduction of cells with a Trim46-positive process in the subpopulation of cells containing  $\leq 1$  centriole(s) compared to cells still containing 2 centrioles upon Centrinone-B treatment (Fig 2D). Accordingly, Trim46-negative processes were more often observed in centriole-depleted neurons compared to neurons still containing both centrioles upon Centrinone-B treatment, whereas this distinction was not observed in control (Fig EV2F). To control for possible off-target effects of Centrinone-B, we used an additional approach to induce centriole loss based on genetic manipulation of

SAS6, an important regulator of centriole duplication and a component of the centriole cartwheel structure (Nakazawa *et al*, 2007). Transducing human iPSC-derived NSCs with CRISPR/Cas9 SAS6 gRNA knockout lentivirus (SAS6 KO) for five days resulted in a significant reduction of centriole numbers (Fig EV2G and H). Axonal appearance of Trim46 was significantly reduced in neurons transduced with SAS6 KO lentivirus, thereby confirming our previous finding (Fig EV2I and J). Centriole depletion did not seem to affect the overall Trim46 expression levels in neurons, as no clear differences were found upon Centrinone-B treatment with Western blot analysis (Fig EV2K). Another important protein that undergoes axonal sorting is the major AIS scaffold AnkG. In contrast to Trim46, we observed no changes in axonal appearance of AnkG upon Centrinone-B-induced centriole depletion (Fig 2E). Consistently, cells containing  $\leq 1$  centriole(s) showed reduced Trim46 colocalization at AnkG-positive axonal structures (Fig 2F). To control for possible post-differentiation effects of PLK4 inhibition unrelated to centriole number, we investigated if axonal targeting of Trim46 was affected when applying Centrinone-B treatment after neuronal differentiation. Treating neurons with Centrinone-B three days after neuronal induction, which we previously reported as a time point in which most neurons are differentiated but not yet polarized, did

not affect Trim46 appearance at axons or at AnkG-positive structures at later stages (Fig EV2L and M) (Lindhout *et al*, 2020). Together, these data suggest that centrosomes are important for the targeting of Trim46, but not AnkG, to axons during early stages of neuronal development.

### Centriole loss leads to immature action potential firing

The axonal targeting of Trim46 and AnkG is required to assemble the AIS, the highly specialized structure essential for mature and efficient AP firing. Thus, we assessed if the observed differential effects on axon protein targeting upon centriole depletion correlate with changes in AP properties. We performed whole-cell patch clamp recordings of control or Centrinone-B-treated neurons of 7–14 days, which coincides with early axon development. To measure neuronal excitability, we determined the number of APs fired with increasing somatic current injection (steps of 5 pA; 400 ms) (Fig 2G). In Centrinone-B-treated cultures, ~17% of neurons did not fire APs, whereas this was only ~3% in control cultures (Fig 2H and I). Of the firing neurons, there were less Centrinone-B-treated neurons that fired multiple APs compared to control. Neurons that did not fire APs did generate small peaks upon current stimulation, indicating the opening of sodium channels, but did not generate a positive feedback to rapidly increase the membrane potential as is characteristic of APs. In addition, neurons treated with Centrinone-B did not display a progressive maturation of AP properties from day 10 to day 14, as was observed in control neurons (Figs 2J, and EV2N and O). APs fired by Centrinone-B-treated neurons appeared more immature, as they were wider, had smaller amplitudes and smaller after-hyperpolarizations (Figs 2K–M, and EV2N and O). In Centrinone-B-treated neurons, the input resistance was also higher, but membrane potential did not differ from control (Fig EV2O–Q). Although AP threshold was not affected by Centrinone-B treatment (Fig 2M), maximum sodium currents were significantly smaller in Centrinone-B-treated neurons (Fig 2N). To control for centriole-unrelated effects of PLK4 inhibition, we tested the effect of Centrinone-B treatment after differentiation on action potential firing. When Centrinone-B was added post-differentiation, we did not observe a difference in AP amplitude and half-width in neurons of 13–14 days (Fig EV2R and S). Together, the electrophysiology recordings from Centrinone-B-treated neurons show more immature AP firing and reduced sodium currents, thereby highlighting the functional relevance of centrosome-mediated control mechanisms during early stages of neuronal development.

### Centriole depletion results in reduced expression of growth cone proteins

Our observations showed that the centriole-depleted NSCs develop into neurons with structural and functional perturbations in axon development. Next, we aimed to quantify effects of centriole depletion during axon specification with unbiased profiling. Therefore, we performed mass spectrometry-based quantitative proteomics analysis on days 1, 3, and 7, which generally corresponds with developmental stage 1, onset of stage 2, and onset of stage 3, respectively (Lindhout *et al*, 2020). We compared the proteome dynamics during early neurodevelopment of replicates of Centrinone-B-treated and control neurons (Fig EV3A, DATASET EV1). Centrinone-B

treatment did not markedly alter the relative protein expression over time (Fig 3A). The protein expression profile of control neurons showed a developmental shift, which corresponds to the transitions from stage 1 to stage 2, and from stage 2 to stage 3 (Fig EV3B). Protein expression of centriole-depleted neurons largely follows the same trend (Fig EV3C). In both populations, proteins considered specific for NSCs are downregulated at days 3 and 7 (e.g., Ki67, nestin, Otx, Notch1), whereas neuronal proteins are upregulated (e.g., Stathmin1, Map2, doublecortin, Tub $\beta$ 3) (Fig EV3D). The onset of stage 3 marks axon specification, and indeed, we observed strong upregulation of the axonal proteins Trim46 and Tau at day 7, which was not affected by Centrinone-B treatment (Fig 3B). Expression of the growth cone proteins Basp1, Gap43, and Marcks was increased at day 3 in controls as well as Centrinone-B-treated neurons. This upregulation was even stronger at day 7 in control neurons, but was markedly suppressed in the centriole-depleted neurons (Figs 3C and EV3D). Together, the quantitative proteome analysis shows that treatment with Centrinone-B does not dramatically alter the protein expression profile during early stages of neurodevelopment, providing a successful global quality control of Centrinone-B-treated cells. However, these results indicate a specific effect on growth cone proteins upon depletion of centrioles.

### Centriole depletion affects neurite growth cone morphology

Next, we examined if the reduced expression of growth cone proteins resulted in defects of axonal growth cone morphology. We found that in control neurons the size of growth cones is relatively large early in development and decreases over time (Fig 3D and E). Growth cones of neurons treated with Centrinone-B remained smaller at day 5, and their size decreased even further later in development. As microtubules are essential components to shape growth cones, we investigated whether manipulation of the microtubule cytoskeleton mimicked the effect of centriole depletion by Centrinone-B treatment on growth cone size (Dent *et al*, 2011). Indeed, treatment with Nocodazole, a microtubule destabilizer, also resulted in smaller growth cones already at day 5 (Fig 3D and E). Interestingly, Nocodazole treatment did not show an additional effect on growth cone size in centriole-depleted neurons, which suggests similar underlying mechanisms. To study the effect of centriole depletion on growth cones more specifically, we categorized three subtypes: fan-like, torpedo-like, and bulb-like (Fig 3F) (van der Vaart *et al*, 2013). We found a majority of fan-like growth cones at day 5, which shifted to more torpedo-like and bulb-like growth cones as axons matured (Fig 3G). Neither Centrinone-B nor Nocodazole treatment altered the relative abundance of these types of growth cones. However, Centrinone-B as well as Nocodazole treatment did result in significantly smaller fan-like growth cones at day 5, which in control neurons are considerably larger than torpedo- and bulb-like growth cones (Fig 3H). This effect was distinct for fan-like growth cones, as the sizes of torpedo-like and bulb-like growth cones were unaffected, which suggests that the observed decrease of growth cone size is specifically due to affected fan-like growth cones (Fig 3E and H). The actin cytoskeleton is another important cytoskeletal component at growth cones and was previously found to be controlled by microtubules as well as centrosome activity in dissociated rodent neurons (Zhao *et al*, 2017; Meka *et al*, 2019). Here, we observed no changes in local levels of F-actin at

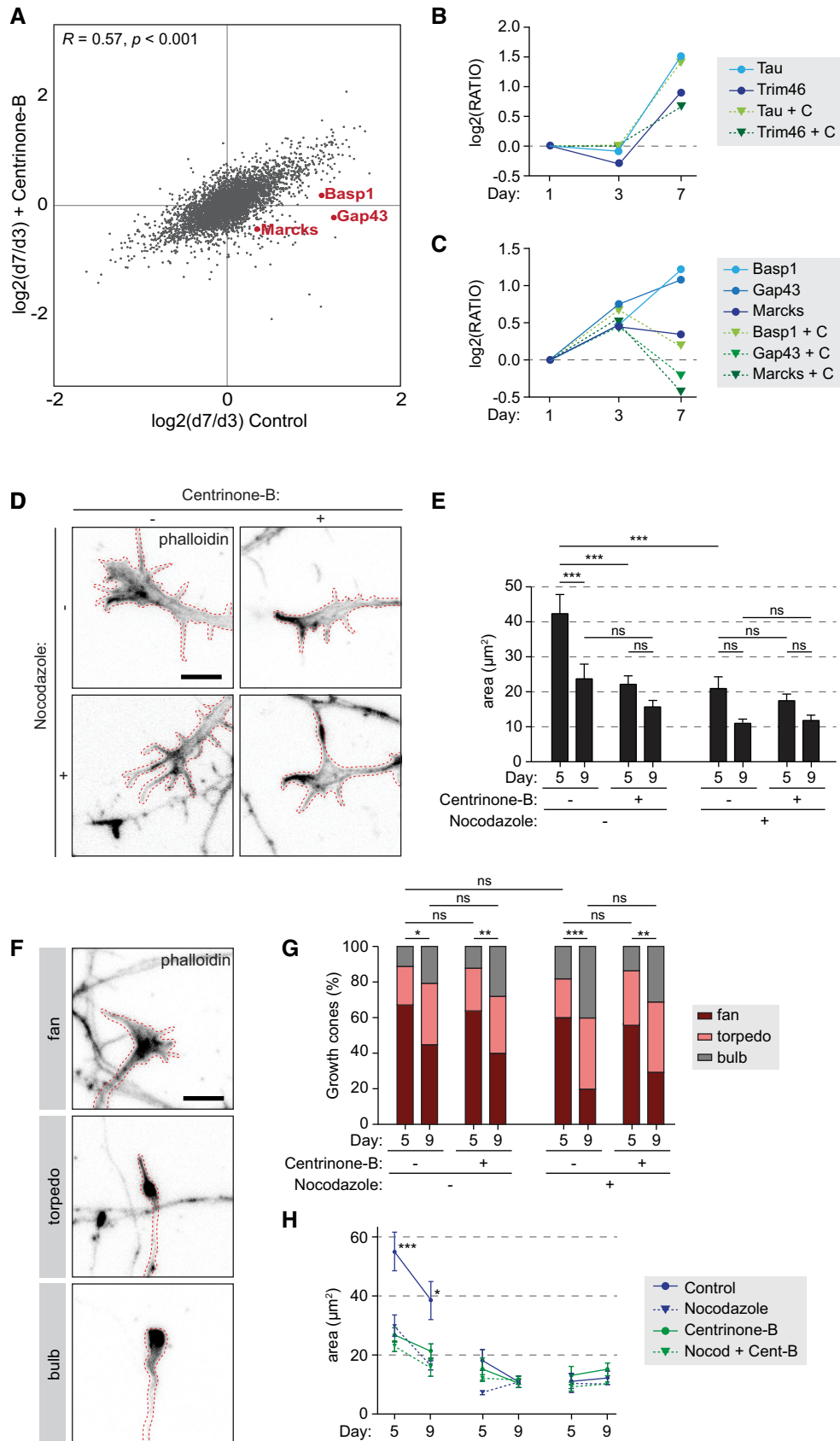


Figure 3.



**Figure 3. Centriole loss in NSCs is accompanied with changes in neurite growth cone morphology.**

- A Correlative plot of changes in protein abundance between control neurons and neurons treated with Centrinone-B (day 7/day 3). Pearson's correlation  $R = 0.5716$ ,  $P < 0.001$ . Specific, significantly changing growth cone proteins highlighted in red.
- B Protein abundance profile over time for axon-related proteins Trim46 and Tau in control neurons and neurons treated with Centrinone-B (+C).
- C Protein abundance profile over time for growth cone-related proteins Basp1, Gap43, and Marcks in control neurons and neurons treated with Centrinone-B (+C).
- D Representative images of fan-like growth cones at day 5 of control and Centrinone-B-treated neurons with or without Nocodazole treatment. Growth cones are visualized by immunostaining for phalloidin. Scale bar = 5  $\mu\text{m}$ .
- E Quantifications of the average area ( $\mu\text{m}^2$ ) of growth cones of control and Centrinone-B-treated neurons, with or without Nocodazole treatment, at different time points.  $n = 25\text{--}83$  growth cones in three independent experiments.
- F Representative images of different growth cone morphological categories: fan-like, torpedo-like and bulb-like. Scale bar = 5  $\mu\text{m}$ .
- G Quantifications of the ratios of different subtypes (fan-like, torpedo-like, bulb-like) of growth cones of control and Centrinone-B-treated neurons, with or without Nocodazole treatment, at different time points.
- H Quantifications of the average area ( $\mu\text{m}^2$ ) of different subtypes (fan-like, torpedo-like, bulb-like) of growth cones of control and Centrinone-B-treated neurons, with or without Nocodazole treatment, at different time points.  $n = 5\text{--}55$  growth cones in three independent experiments.

Data information: Data represent mean  $\pm$  SEM. One-way ANOVA including Tukey's *post hoc* analysis (E), Chi-square test including *post hoc* analysis with Bonferroni correction (G), One-way ANOVA including Sidak's *post hoc* analysis (H). \*\*\* $P < 0.001$ , \*\* $P < 0.005$ , \* $P < 0.05$ , ns  $P \geq 0.05$ .

growth cones, suggesting that the reduced size of fan-like growth cones is not caused by changes in F-actin levels in growth cones (Fig EV3E). Together, these results suggest that centriole depletion causes growth cone morphology defects during axon outgrowth, presumably through microtubule-mediated mechanisms.

### Centriole depletion perturbs microtubule reorganization in developing axons

To gain more insight into the potential role of centrosomes on the unique organization of the axonal microtubule cytoskeleton, marked by a uniform organization of plus-end out microtubules, we studied the effect of centriole loss on the microtubule remodeling processes during development. We systematically analyzed plus-end dynamics and orientations of microtubules in axons and dendrites on day 7 and 13, which coincide with the onset of stage 3 and late stage 3, respectively (Lindhout *et al*, 2020). For the analysis at axons, we measured both proximal and distal regions, as we previously reported that axon development follows a distal-to-proximal reorganization during this time window in human iPSC-derived neurons (Lindhout *et al*, 2020). We used two-color live-cell imaging to visualize neurite morphology and microtubule plus-end tracking proteins (MT+TIPs) in control neurons and Centrinone-B-treated neurons (Fig 4A, MOVIE EV1). The direction of moving MT+TIPs is used as read-out for microtubule orientations, as anterograde and retrograde movement of MT+TIPs mark plus-end out and minus-end out microtubules, respectively. On day 7, the percentage of Centrinone-B-treated neurons with a uniform microtubule polarity, which is a hallmark of mature axons, is similar to control neurons in both proximal and distal axons (Figs 4B and C, and EV4A and B). Similarly, the numbers of anterogradely and retrogradely growing MT+TIPs are not changed upon Centrinone-B treatment (Figs 4D and E, and EV4D and E). However, on day 13 the proportion of neurons with uniform microtubules in the distal axon was significantly reduced by Centrinone-B treatment compared to control neurons (Fig 4B and F). Microtubule polarity was specifically affected in the distal axon, which represents the most mature axonal stage, as no difference was observed in the proximal axons and the dendrites of control neurons and Centrinone-B neurons (Fig EV4A–C, F–H). This indicates that centriole depletion prevents neurons from retaining the characteristic uniform plus-end out microtubule organization during axonal

development. Furthermore, Centrinone-B-treated neurons show more MT+TIP movement, in particular for anterograde moving MT+TIPs, which suggests a global increase of microtubule dynamics (Fig 4G and H). An increase in the number of MT+TIPs is also observed in the proximal axon at day 13, but not in the dendrites (Fig EV4D, E, I, J). The speed and run length of growing MT+TIPs was consistent between control neurons and Centrinone-B-treated neurons at dendrites as well as proximal and distal axons across both time points (DATASET EV2). Imaging of MT+TIPs only provides information about the dynamic ends of microtubules, but does not account for stabilized microtubules. Thus, we next aimed to analyze the microtubule orientations of the total axonal microtubule network, including both stable and dynamic microtubules. This was addressed by combining our approach with laser severing to generate new microtubule ends by cutting microtubules with a short-pulsed laser, which triggers newly formed MT+TIPs (Fig 4I and J, MOVIE EV2) (Yau *et al*, 2016). Consistent with previous findings, we observed a marked  $\sim 40\%$  reduction of neurons with a uniform plus-end microtubule organization in distal axons with Centrinone-B treatment following laser severing of microtubules, whereas no significant changes were observed in proximal axons (Figs 4K, L, O, and EV4K, L, M). At distal axons, the number of retrograde comets was significantly increased upon Centrinone-B treatment, whereas anterograde comets were unaffected, suggesting that centriole loss is accompanied with more stable minus-end out microtubules at developing axons (Fig 4M, N, P, Q). As expected, the number of anterograde and retrograde comets was not changed at proximal axons and dendrites with Centrinone-B treatment (Fig EV4N, O, P, Q, R). To control for PLK4 inhibition effects in postmitotic neurons unrelated to centriole number, we analyzed the microtubule organization in distal axons at day 13 in neurons treated with Centrinone-B after differentiation and observed no significant differences compared to control (Fig EV4S, T, U). Together, these data suggest that centrosomes are important for the unique axon-specific reorganization toward uniform plus-end out microtubules (Fig 4R).

## Discussion

Understanding the role of centrosomes during axon development has been a long-lived question and is still an ongoing debate. Early

reports already suggested that microtubule nucleation is important for axon formation and outgrowth in dissociated rodent neurons and proposed that centrosomes could play an important role in axon development (Ahmad *et al*, 1994). Indeed, in *Drosophila* neurons,

centrosome dysfunction affected axon formation and outgrowth (de Anda *et al*, 2005). In dissociated rodent neuron cultures, centrosome positioning was found to correlate with sites of newly emerging axons (Zmuda & Rivas, 1998; de Anda *et al*, 2005). However,

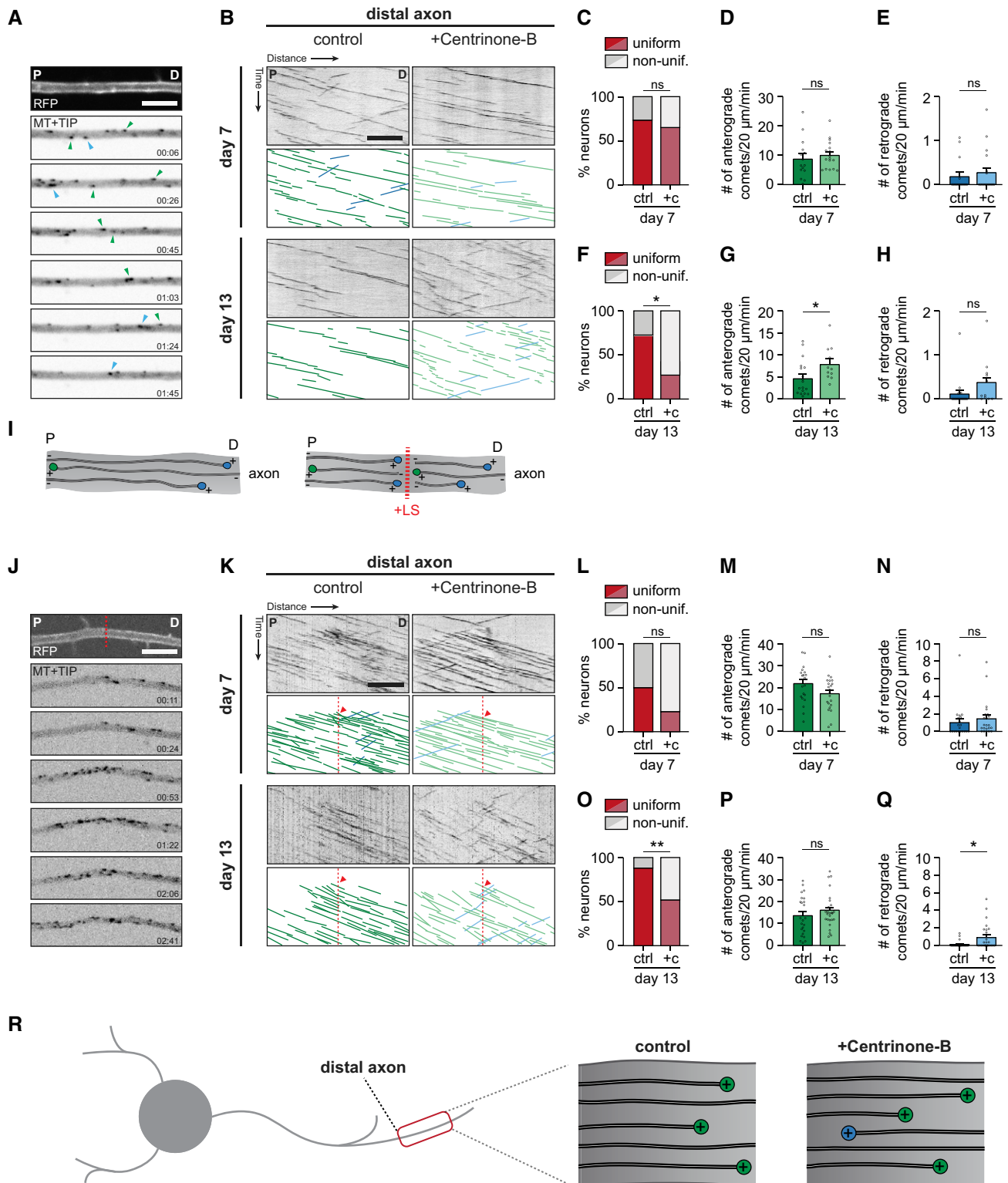


Figure 4.

**Figure 4. Centriole loss restrains microtubule remodeling during early axon development.**

- A Example stills from a spinning-disk time-lapse recording of a neurite transfected with mRFP and GFP-MT+TIP. The top panel is a still of a neurite in mRFP, showing neurite morphology. The other panels show moving GFP-MT+TIP comets pointing in either an anterograde direction (green arrowheads) or retrograde direction (blue arrowheads). P indicates the proximal direction and D the distal direction of the neurite. Timestamp in minutes:seconds given on bottom right. Scale bar = 5  $\mu$ m.
- B Kymographs and schematic representations of time-lapse recordings of the distal axon as shown in (A), for different time points (day 7; day 13) and conditions (control; Centrinone-B). Scale bar = 5  $\mu$ m.
- C Quantifications of the percentage of neurons exhibiting uniform, or non-uniform comet orientations in the anterograde direction in the distal axon at day 7.  $n = 15-17$  cells in four independent experiments.
- D Quantifications of the number of comets per minute moving in the anterograde direction in the distal axon at day 7.  $n = 15-17$  cells in four independent experiments.
- E Quantifications of the number of comets per minute moving in the retrograde direction in the distal axon at day 7.  $n = 15-17$  cells in four independent experiments.
- F Quantifications of the percentage of neurons exhibiting uniform, or non-uniform comet orientations in the anterograde direction in the distal axon at day 13.  $n = 11-18$  cells in four independent experiments.
- G Quantifications of the number of comets per minute moving in the anterograde direction in the distal axon at day 13.  $n = 11-18$  cells in four independent experiments.
- H Quantifications of the number of comets per minute moving in the retrograde direction in the distal axon at day 13.  $n = 11-18$  cells in four independent experiments.
- I Schematic representation of microtubule laser-severing (LS) experiments.
- J Example stills from a spinning-disk time-lapse recording of a neurite transfected with mRFP and GFP-MT+TIP. Red line denotes the location of LS. Scale bar = 5  $\mu$ m.
- K Kymographs and schematic representations of time-lapse recordings of the distal axon as shown in (J) following LS, for different time points (day 7; day 13) and conditions (control; Centrinone-B). Red line and red arrowhead denote location and time of LS. Scale bar = 5  $\mu$ m.
- L Quantifications of the percentage of neurons exhibiting uniform, or non-uniform comet orientations in the anterograde direction in the distal axon following LS at day 7.  $n = 20-22$  neurons in three independent experiments.
- M Quantifications of the number of comets per minute moving in the anterograde direction in the distal axon following LS at day 7.  $n = 20-22$  cells in three independent experiments.
- N Quantifications of the number of comets per minute moving in the retrograde direction in the distal axon following LS at day 7.  $n = 20-22$  cells in three independent experiments.
- O Quantifications of the percentage of neurons exhibiting uniform, or non-uniform comet orientations in the anterograde direction in the distal axon following LS at day 13.  $n = 24-27$  neurons in three independent experiments.
- P Quantifications of the number of comets per minute moving in the anterograde direction in the distal axon following LS at day 13.  $n = 24-27$  cells in three independent experiments.
- Q Quantifications of the number of comets per minute moving in the retrograde direction in the distal axon following LS at day 13.  $n = 24-27$  cells in three independent experiments.
- R Schematic representation of the proposed orientation of microtubules in the distal axon in control conditions, and following Centrinone-B treatment.
- Data information: Data represent mean  $\pm$  SEM. Chi-square test (C, F, L, O), unpaired *t*-test (D, E, G, H, M, N, P, Q); \*\* $P < 0.005$ , \* $P < 0.05$ , ns  $P \geq 0.05$ .

centrosome removal in polarized neurons did not affect further axon outgrowth in dissociated rodent neurons, but the role of axon specification, the first step of axon formation, has remained largely unexplored (Stiess *et al*, 2010). This is mostly due to technical challenges that prevent investigation of the early molecular processes that drive axon specification. Here, we used human iPSC-derived neurons to investigate centrosome function during axon specification, as human neurons undergo a significant protracted development compared to classically used, non-human model systems, thereby increasing the temporal resolution to study these processes. We uncovered that centrosomes are important for microtubule remodeling during early axon development in human neurons and are thereby setting the foundation for subsequent axon maturation and functioning.

#### Trim46 localizes at the centrosome and AIS at different stages of neuronal development

Trim46 was identified as a microtubule-associated protein localizing to the proximal part of the AIS, where it locally binds and stabilizes parallel microtubule bundles (van Beuningen *et al*, 2015). In this study, we report the uncharacteristic localization of Trim46 near centrosomes in unpolarized neurons, which is shifted toward their characteristic localization at axons during neuronal polarization. Interestingly, a similar developmental shift was previously reported for NDEL1, a dynein regulating protein (Kuijpers *et al*, 2016). It remains unknown if there are additional microtubule-associated proteins showing the developmental translocation from centrosomes

to axons. Remarkably, the axonal accumulation of Trim46 was perturbed upon centriole removal, likely signifying a differentially organized axonal microtubule network. Consistent with this idea, we observed less parallel plus-end out microtubules in axons upon centriole loss. Previous *in vitro* reconstitution assays revealed that Trim46 binding favors bundles of parallel oriented microtubules (Freal *et al*, 2019). High-resolution imaging showed that Trim46 appeared as small punctae surrounding the outer layer of the pericentriolar material and did not coincide with previously resolved structures of centrosomal proteins (Mennella *et al*, 2012). Considering that Trim46 is a microtubule-associated protein favoring parallel microtubule bundles, we speculate that Trim46 localizes to the starting points of centrosomal microtubule arrays nucleated from yTuRCs at the PCM (Freal *et al*, 2019). Hence, as major MTOCs, centrosomes likely represent the site with the highest occurrence of parallel oriented microtubules in cells with a radial microtubule network. The function of centrosome-associated Trim46 remains elusive, although it is tempting to speculate that it plays a role in stabilizing the parallel oriented microtubules, consistent with its previous reported function in axons (van Beuningen *et al*, 2015).

#### Dissecting the mechanistic role of centrosomes in axon development

Our data indicate that the centrosome is a critical regulator of axonal microtubule organization during early neuronal development. First, we show that centrosomes display microtubule-

organizing functions during the process of axon specification, and not in polarized neurons. This illustrates the potential of centrosomes, as main MTOCs, to contribute to microtubule remodeling during onset of axon development. Second, centriole loss had distinct effects on AIS assembly and function, as illustrated by the absence of microtubule-binding Trim46 proteins, and more immature AP firing and reduced sodium currents. It is likely that the perturbed centrosome-mediated microtubule remodeling underlies the observed functional defects. Third, at earlier developmental stages, centriole loss affected growth cone formation, which was mimicked by drug treatments that cause microtubule destabilization. Fourth, we found that centriole loss results in a marked delay in the axon-specific uniform plus-end out microtubule reorganization. The effects of centriole loss on axon formation in this study were measured by correlating experimental observations induced by Centrinone-B treatment with the number of centrioles in cells whenever this was technically feasible. Other effects of Centrinone-B treatment on axon formation were measured in a mixed neuron population of which approximately half of the cells lost at least one centriole. With this approach, we cannot exclude that neurons containing one centriole may to some extent still exhibit centrosomal MTOC functions. However, our data clearly show that developmental axon perturbations are identified in the mixed neuron population generated by Centrinone-B treatment, which is indicative of the large effect sizes of the reported findings and also implies that single centriole loss is sufficient to at least partially perturb centrosome functions. The precise mechanism of how centrioles mediate axonal microtubule rearrangements in human iPSC-derived neurons remains largely unclear. Developmental decline of centrosomal microtubule nucleation is a controlled process occurring after axon specification (Stiess *et al*, 2010). Perturbing this controlled timing by removing centrioles prior to axon specification may result in a differentially organized microtubule network in young neurons. Interestingly, a relative increase in acentrosomal microtubules was found in epithelial cells subjected to Centrinone-B-induced centriole loss (Martin *et al*, 2018). We speculate that premature centriole loss may promote acentrosomal microtubule nucleation in axons and thereby increase minus-end out microtubules. Alternatively, non-microtubule functions might be at play, as centrosomes were also found to play a role in functions such as intracellular signaling, protein homeostasis, and organizing the actin cytoskeleton that are relevant for neurodevelopment (Conduit *et al*, 2015; Farina *et al*, 2016; Vora & Phillips, 2016; Meka *et al*, 2020). However, it remains unknown to what extent these functions contribute to axon formation. Altogether, our data show that centrosomes are critical for setting-up the correct microtubule organization during axon specification, which is important for subsequent microtubule remodeling in growing axons.

### Centrosome dysfunction results in premature differentiation and repressed axon development

Neurodevelopment is orchestrated by a highly temporal controlled sequence of events. Centrosome dysfunction significantly perturbs this coordinated timing resulting in microcephaly disorders (Nano & Basto, 2017). These reduced brain sizes are mostly attributed to a reduction of the NSC pool due to premature differentiation and cell death (Nano & Basto, 2017). Here we show that NSCs prematurely

differentiate into neurons when centrosome function is impaired, consistent with previous reports in human iPSC-derived cerebral organoids (Lancaster *et al*, 2013). Previous studies did not reveal whether these prematurely differentiated neurons subsequently follow normal developmental timing and are able to grow functional axons. Here we found reversed timing effects on axon development in prematurely differentiated neurons, as centriole loss perturbed microtubule remodeling during axon formation. The structural axon developmental defects were also accompanied by compromised axon function, as demonstrated by impaired AP firing and reduced sodium currents with centrosome dysfunction. Presumably, the observed functional axon defects are the result of a perturbed organization of the axonal microtubule network in centriole-depleted neurons. Setting-up the distinct microtubule organization in axons and dendrites is an important aspect of neuron polarity, and altering this process might have severe consequences for polarized cargo transport and further neurodevelopment (van Beuningen & Hoogenraad, 2016). In the brain, correct timing of axonal outgrowth during neurodevelopment is key, as axon pathfinding is steered by gradients of chemical attractants or repellents that are highly spatiotemporally controlled (Stoeckli, 2018). We therefore speculate that centrosome-mediated alterations in axon development may significantly affect axon targeting and neuronal innervation *in vivo*. To this end, it would be interesting to direct future research in addressing the long-term functional consequences of an altered axonal microtubule network due to centrosome dysfunction.

## Materials and Methods

### Human iPSC-derived neuron culture

Human iPSC-derived neuronal stem cells (ax0016, Axol Bioscience) were purchased, expanded, and subjected to neuronal differentiation and maintenance as previously prescribed (Lindhout *et al*, 2020). In brief, for expansion of human iPSC-derived NSCs, cells were plated on SureBond-coated plastic wells of a six-well plate and kept in Neuronal Plating-XF medium (ax0033, Axol Bioscience) at 37°C with 5% CO<sub>2</sub>. On the next day, medium was replaced by Neuronal Expansion-XF Medium supplemented with EGF (20 ng/ml; AF-100-15, Peprotech) and FGF (20 ng/ml; 100-18B, Peprotech), which was refreshed every two days. For cell passaging, cells were washed once with PBS, dissociated with Unlock (ax0044, Axol Bioscience), and plated and maintained on pre-coated wells as described above. NSCs were passaged maximum three times prior to neuronal differentiation. For neuronal differentiation, human iPSC-derived NSCs were plated on ReadySet/SureBond-coated glass coverslips and kept in Neuronal Plating-XF medium (ax0033, Axol Bioscience) at 37°C with 5% CO<sub>2</sub>. Cells were plated at a density of ~40 k cells per well for control and ~60 k cells per well or Centrinone-B-treated conditions, to compensate for the decreased proliferating rates induced by centrosome dysfunction. Unless stated differently, neuronal differentiation was induced two days after plating by replacing the medium to Neuron Differentiation-XF Medium (ax0032, Axol Bioscience), and differentiated neurons were next maintained in Neuronal Maintenance-XF Medium, half of the medium was refreshed every three days (ax0034, Axol Bioscience).

### Primary rat hippocampal neuron, HeLa, and IMCD3 cell culture

Dissociated rat hippocampal neuron cultures were prepared as previously described (Lindhout *et al*, 2019). In brief, neurons were obtained from embryonic day 18 rat pups, plated on poly-L-lysine/laminin-coated coverslips (100 k/well), and kept in Neurobasal medium (NB) supplemented with 2% B27, 0.5 mM glutamine, 16.6  $\mu$ M glutamate, and 1% penicillin/streptomycin at 37°C with 5% CO<sub>2</sub>. HeLa or IMCD3 cells were plated on plastic for expansion and 18 mm coverslips for experiments and kept in DMEM/Ham's F10 (50%/50%) medium supplemented with 10% FCS and 1% penicillin/streptomycin at 37°C with 5% CO<sub>2</sub>.

### Pharmacological treatments

For centriole loss experiments, cells were treated with Centrinone-B (500 nM; HY-18683, MedChemExpress) 1 h after plating, or 5 days after plating for late post-differentiation Centrinone-B treatment experiments, and treatment was continued with every following medium change to prevent unintentional wash-out. For growth cone experiments, if indicated, cells were treated for 24 h with 20 nM Nocodazole (Sigma-Aldrich, M1404) prior to fixation.

### Lentiviral infection

Constructs expressed by lentiviral infections in this study are FUGW-GFP (Addgene #14883, (Lois *et al*, 2002)) and Marcks-tagRFP-T-pIres-GCN4-MacF18. Cloning of Marcks-tagRFP-T-pIRES-GCN4-MacF18 is described previously (Yau *et al*, 2014). In short, the construct was subcloned into the lentiviral vector pSIN-TRE-mSEAP-hPGK-rtTA2sM2 (kind gift from Dr. Didier Trono, Ecole Polytechnique Fédérale de Lausanne, Lausanne, Switzerland) in which the PGK promoter was substituted by the neuron-specific synapsin promoter. Lentiviral particles were generated as described previously (Yau *et al*, 2014). Cells were transduced with lentivirus 0.5–2 h after plating. The doxycycline-dependent expression was induced two days before imaging by supplementing the medium with 500 ng/ml doxycycline. For SAS-6 knockout lentivirus production, HEK293T cells were transfected using polyethylenimine (PEI, Polysciences) with second-generation LV packaging plasmids (psPAX2 and 2MD2.G) and a lentiCRISPR-KO-P2A-mCherry plasmid containing SpCas9-P2A-mCherry and the desired target sequences at a 1:1:1 molar ratio. 48 h after transfection, supernatant was harvested, briefly centrifuged to remove cell debris, and concentrated using Amicon Ultra 15 100K MWCO columns (Millipore). LentiCRISPR-KO-P2A-mCherry was created by exchanging the puromycin resistance gene to mCherry in the lentiCRISPR-KO plasmid, which was a gift from Feng Zhang (Shalem *et al*, 2014). Target sequences (SAS-6: 5' CCTGCAACGGGACTA GTTGG 3'; KO control: 5' CCGGGTCTTCGAGAAGACCT 3' (Willems *et al*, 2020)) were inserted in lentiCRISPR-KO-P2A-mCherry between BsmBI sites. Attempts to examine SAS-6 expression levels upon transducing hiPSC-derived NSCs for 5 days with SAS6 and control KO lentiviral constructs using Western Blot analysis and immunofluorescence did not succeed, as the signals observed with the SAS-6 antibody (sc-81431, Santa Cruz) did not coincide with the expected SAS-6 molecular weight and localization in human iPSC-derived NSCs.

### Antibodies

The following primary antibodies were used in this study: mouse-IgG1 anti- $\gamma$ -tubulin (1:500; T6557, Life Technologies), mouse-IgG2a anti-Centrin (1:300; 20H5, Millipore), rabbit anti-Ki67 (1:500; ab92742, Abcam), chicken anti-MAP2 (1:2000; ab5392, Abcam), rabbit anti-Trim46 (1:500; homemade, (van Beuningen *et al*, 2015)), mouse-IgG1 anti-nestin (1:200; MAB5326, Millipore), mouse-IgG1 anti- $\alpha$ -tubulin (1:1,000; T-5168, Sigma), rabbit anti-pericentrin (1:500; 923701, BioLegend), mouse-IgG1 anti-AnkG (1:200; 33-8800, Life Technologies), mouse-IgG2b anti- $\beta$ 3-tubulin (1:400; T8660, Sigma). The following secondary antibodies were used in this study: anti-chicken Alexa 405 (ab175675, Abcam), anti-rabbit Alexa 488 (A11034, Life Technologies), anti-chicken Alexa 488 (A11039, Life Technologies), anti-mouse Alexa 488 (A11029, Life Technologies), anti-mouse-IgG1 Alexa 488 (A21121, Life Technologies), anti-rabbit Alexa 568 (A11036, Life Technologies), anti-mouse Alexa 568 (A11031, Life Technologies), anti-mouse-IgG1 Alexa 594 (A21125, Life Technologies), anti-mouse-IgG2a Alexa 594 (A21135, Life Technologies), anti-chicken Alexa 647 (A21449, Life Technologies), anti-rabbit Alexa 647 (A21245, Life Technologies) anti-mouse Alexa 647 (A21236, Life Technologies), anti-mouse-IgG2a Alexa 647 (A21241, Life Technologies), phalloidin Alexa 647 (A22287, Life Technologies). The following antibodies were used for Western blotting: mouse anti-Actin (1:10,000; MAB1501R, Merck), guinea pig anti-Trim46 (1:1,000; 377005, SySy), goat anti-mouse IRDye680CW (1:20,000, LI-COR), and goat-anti-guinea pig IRDye800LT (1:5,000, LI-COR).

### Immunofluorescence

For centrosomal stainings, cells were fixed for 10 min in methanol at  $-20^{\circ}$ C. For other experiments, cells were fixed for 10 min in PBS with 4% formaldehyde/4% sucrose (for neurons) or 10 min in PBS with 4% formaldehyde (for non-neuronal cells) at room temperature. After fixation, cells were washed three times with PBS. Fixed cells were sequentially incubated with primary and secondary antibodies diluted in gelate dilution buffer (GDB; 0.2% BSA, 0.8 M NaCl, 0.5% Triton X-100, 30 mM phosphate buffer, pH 7.4). Cells were washed three times with PBS after every antibody incubation, and coverslips were mounted using Vectashield mounting medium (Vector laboratories) with or without DAPI.

### Microscopy

Confocal microscopy of fixed cells was performed on a LSM700 confocal laser-scanning microscope (Zeiss) equipped with the following objectives: (i) a Plan-Apochromat 63 $\times$  NA 1.4 oil DIC; (ii) a EC Plan-Neofluar 40 $\times$  NA 1.3 Oil DIC; and (iii) a Plan-Apochromat 20 $\times$  NA 0.8 objective. Dual-color gated STED (gSTED) imaging was performed on a Leica TCS SP8 STED 3X microscope using a HC PL APO 100 $\times$ / N.A. 1.4 oil immersion STED WHITE (Leica 15506378) objective in 2D STED configuration (vortex phase mask). The 488, 590, and 647 nm wavelengths of pulsed white light laser (80 MHz) were used to excite Alexa 488-labeled  $\gamma$ -tubulin, Alexa 594-labeled Centrin, and Alexa647-labeled Trim46, respectively. Alexa 594 and Alexa 647 were depleted with the 775 nm pulsed depletion laser and an internal Leica HyD hybrid detector (100%

gain) with a time gate of  $0.3 \leq t_g \leq 6$  ns was used. 3D STED imaging of microtubules was performed using HC PL APO 93  $\times/1.30$  GLYC motCORR STED (Leica 15506417) glycerol-immersion objective with corrective collar. Abberior STAR 635P dye was excited with 633 nm white light laser and depleted with 775 nm STED laser. We used a combined depletion PSF light path consisting of a mixture 60% Z-donut and 40% vortex phase mask, providing approximately isotropic resolution. Spinning-disk confocal microscopy for live-cell imaging was performed on an inverted microscope Nikon Eclipse Ti-E, which was equipped with a spinning-disk-based confocal scanner unit (CSU-X1-A1, Yokogawa), an ASI motorized stage with the piezo plate MS-2000-XYZ (ASI), and the perfect focus system (Nikon). We used the following cameras: (i) a Photometric Evolve Delta 512 EMCCD camera controlled by the MetaMorph 7.8 software (Molecular Devices), or (ii) a Photometric PRIME BSI sCMOS camera (version USB 3), controlled by the MetaMorph 7.10 software (Molecular Devices). We used the 491 nm 100 mW Calypso (Cobolt) and 561 nm 100 mW Jive (Cobolt) lasers as light sources. For imaging of GFP-tagged proteins, we used an ET-GFP filter set (49002, Chroma), for imaging of proteins with tagRFP we used an ET-mCherry filter set (49008, Chroma). For live-cell imaging with photoablation, we used an ILas system (Roper Scientific France/PICT-IBiSA, Institut Curie, currently Gataca Systems) mounted on the Nikon Eclipse microscope described above. We used a 355 nm passively Q-switched pulsed laser (Teem Photonics) for the photoablation, together with the S Fluor 100 $\times$  0.5–1.3 NA oil objective (Nikon). To cut several microtubules simultaneously, we moved the same laser beam along the line positioned perpendicular to several microtubules. All live-cell imaging experiments were performed in full conditioned differentiation (day 5) or maintenance (days 7 and 13) medium for human iPSC-derived neuron cultures (Axol). To keep cells at 37°C with 5% CO<sub>2</sub>, we used a stage top incubator (model INUBG2E-ZILCS, Tokai Hit).

### Image quantification and analysis

#### Determining centrosomal $\gamma$ -tubulin levels

Centrosomal  $\gamma$ -tubulin levels were quantified in stage 1 (day 0; Ki67-positive), stage 2 (day 7; MAP2-positive and axonal Trim46-negative), and stage 3 neurons (day 12; MAP2-positive and axonal Trim46-positive). Centrosomes were identified by co-localization of  $\gamma$ -tubulin and Centrin. A region of interest was manually drawn around centrosomes based on the Centrin signal, and the average  $\gamma$ -tubulin immunofluorescence intensity within this region was measured and corrected for background intensities. The mean intensities of each neurodevelopmental stage were normalized to the mean intensity of stage 1 neurons.

#### Measuring development of neuronal differentiation

To determine the effect of Centrinone-B treatment on neuronal differentiation over time, cells were identified using DAPI staining and scored to be positive or negative for Ki67, MAP2, or  $\beta$ 3-tubulin.

#### Quantifying growth cone morphologies

Growth cone size was measured by manually drawing a region of interest based on phalloidin signal and measuring the area in  $\mu\text{m}^2$ . Growth cones were categorized as fan-like, torpedo-like, or bulb-like based on shape.

### Live-cell imaging

For microtubule dynamics experiments without laser severing, time-lapse acquisition was performed using the 491 nm 100 mW Calypso (200 ms exposure) and 561 nm 100 mW Jive (200 ms exposure) with 1 frame per second (fps) for 5 min, with a Plan Apo VC 60 $\times$  NA 1.4 oil immersion objective (Nikon). 16-bit images were projected onto the EMCCD chip with intermediate lens 2.0X (Edmund Optics) at a magnification of 0.111  $\mu\text{m}/\text{pixel}$  at 60 $\times$ , or onto the sCMOS chip with no intermediate lens at a magnification of 0.150  $\mu\text{m}/\text{pixel}$  at 60 $\times$ . For microtubule dynamics experiments with laser severing, time-lapse acquisition was performed using the 491 nm 100 mW Calypso (50–200 ms exposure) and 561 nm 100 mW Jive (50–200 ms exposure) with 1 fps for 3 min. Selected regions were subjected to photoablation between frame 30 and 31. 16-bit images were projected onto the sCMOS chip with no intermediate lens at a magnification of 0.063  $\mu\text{m}/\text{pixel}$  at 100 $\times$ . For analysis of microtubule plus-end dynamics, kymographs were generated with the FIJI plugin KymoResliceWide v.0.4 (<https://github.com/ekatruckha/KymoResliceWide>), and tracing microtubule growth events were manually traced.

### Electrophysiology

Before the start of each experiment, a 12 mm coverslip with Centrinone-B-treated or control human iPSC-derived neurons (paired cultures of 7–14 days after plating) was placed under the microscope. In the recording chamber, carbogenated (95% O<sub>2</sub>, 5% CO<sub>2</sub>) artificial cerebrospinal fluid (ACSF, in mM: 126 NaCl, 3 KCl, 2.5 CaCl<sub>2</sub>, 1.3 MgCl<sub>2</sub>, 26 NaHCO<sub>3</sub>, 1.25 NaH<sub>2</sub>PO<sub>4</sub>, 20 glucose; with an osmolarity of  $\sim$  310 mOsm/l) was continuously perfused at a rate of approximately 1 ml/min. An extra medium refreshment was conducted one day before recording, to prevent changes in excitability due to acute differences in extracellular osmolarity (Pasantes-Morales, 1996). ACSF was warmed before entering the bath, and the temperature was maintained at 30–32°C. Recording pipettes pulled from thick-walled borosilicate glass capillaries (World Precision Instruments) had a resistance of 4–7 M $\Omega$  and were filled with internal solution (in mM: 140 K-gluconate, 4 KCl, 0.5 EGTA, 10 HEPES, 4 MgATP, 0.4 NaGTP, 4 Na<sub>2</sub>-Phosphocreatine; with pH 7.3 and osmolarity 295 mOsm/l). To facilitate visualization of cells during the experiment and *post hoc*, the internal solution was supplemented with 30  $\mu\text{M}$  Alexa 568 (Thermo Fisher Scientific) and biocytin, respectively. We selected individual neurons with a 60 $\times$  water immersion objective (Nikon NIR Apochromat; NA 1.0) and performed whole-cell somatic patch clamp recordings. During the recordings in both voltage and current clamp, cells were kept at a holding potential of  $-60$  mV. Recordings were acquired with an Axopatch 200B amplifier (Molecular Devices) using pClamp 10 software. Data were analyzed with Clampfit 10.7 software and custom-written MATLAB scripts.

### Mass spectrometry

To obtain sample preparations for mass spectrometry (TMT labeling), biological replicates of control and Centrinone-B-treated human iPSC-derived neurons were harvested at three different time points (days 1, 3, and 7) of differentiation with lysis buffer (8 M urea, 50 mM ammonium bicarbonate (Sigma), EDTA-free protease inhibitor cocktail (Roche)). Lysates were sonicated on ice using

Bioruptor (Diagenode) and cleared by centrifugation at 2,500 g for 10 min. Protein concentration was determined using Bradford assay. From each condition, 100 µg of proteins was reduced (5 mM DTT, 55°C, 1 h), alkylated (10 mM Iodoacetamide, 30 min in the dark), and sequentially digested by LysC (Protein-enzyme ratio 1:50, 37°C, 4 h) and trypsin (Protein-enzyme ratio 1:50, 37°C, overnight). After overnight digestion, samples were acidified with formic acid (final concentration 3%) and resulting peptides were then desalted using Sep-Pak C18 columns (Waters). Samples were subjected to stable isotope TMT-6plex labeling according to manufacturer's instruction (Thermo Fisher Scientific). In brief, peptides were resuspended in 80 µl of 50 mM HEPES buffer, 12.5% ACN with pH 8.5 while TMT reagents were dissolved in 50 µl anhydrous ACN. For labeling, 25 µl of each dissolved TMT reagent was added to the correspondent sample according to the following scheme:

Control human iPSC sample, day 1 = TMT-126 / Centrinone-B human iPSC sample, day 1 = TMT-129.

Control human iPSC sample, day 3 = TMT-127 / Centrinone-B human iPSC sample, day 3 = TMT-130.

Control human iPSC sample, day 7 = TMT-128 / Centrinone-B human iPSC sample, day 7 = TMT-131.

Following incubation at room temperature for 1 h, the reaction was quenched using 5% hydroxylamine. Differentially, TMT-labeled peptides were mixed in equal ratios and dried in a vacuum concentrator. Peptide fractionation, MS analysis, data processing, and bioinformatic analysis of the samples were performed as described before (Lindhout et al, 2020).

### Western blot

Human iPSC-derived control neurons or Centrinone-B-treated neurons were eluted at day 5 in SDS/DTT sample buffer. For Western blot analysis, cell lysates were boiled at 95°C for 10 min and cell lysates were run on 12% SDS-PAGE gels, after which proteins were transferred to nitrocellulose membranes (Bio-Rad) by semi-dry blotting for 1 h at 16 V. Membranes were blocked in 3% bovine serum albumin (BSA) in PBST (PBS supplemented with 0.02% Tween20) for 1 h at room temperature and then incubated with primary antibodies diluted in 3% BSA-PBST at 4°C overnight. Membranes were washed three times with PBST, incubated with secondary antibodies diluted in 3% BSA-PBST for 1 h at room temperature, and washed three times with PBST. Membranes were scanned using an Odyssey Infrared Imaging system (LI-COR Biosciences).

### Statistical analysis

All statistical analyses were performed using GraphPad Prism (version 8.0) software. Statistical tests are described in the corresponding figure legends. *P*-values are annotated as follows: \**P* < 0.05, \*\**P* < 0.01, \*\*\**P* < 0.001, and ns *P* ≥ 0.05.

## Data availability

The mass spectrometry proteomics data have been deposited to the ProteomeXchange Consortium via the PRIDE partner repository with

the dataset identifier PXD020221 (<http://www.ebi.ac.uk/pride/archive/projects/PXD020221>) (Perez-Riverol et al, 2019). The datasets generated and analyzed during the current study are available from the corresponding author upon request.

**Expanded View** for this article is available online.

### Acknowledgements

We thank Dr. Didier Trono for kindly providing the lentiviral vector. This work was supported by the Netherlands Organization for Scientific Research (NWO-ALW-VICI, 865.10.010, CCH), the Netherlands Organization for Health Research and Development (ZonMW-TOP, 912.16.058, CCH), the European Research Council (ERC) (ERC-consolidator, 617050, CCH), and the research program of the Foundation for Fundamental Research on Matter (FOM, #16NEPH05, CJW).

### Author contributions

FWL initiated the study, designed and performed experiments, and wrote the article together with SP, RK and LJH. SP designed and performed experiments for the growth cone analysis, RK provided the microtubule live-imaging data, LJH performed and interpreted the electrophysiology experiments supervised by CJW, RS conducted the mass spectrometry experiments supervised by MA, JJAH performed the biochemistry experiments, NS provided the 2D STED microscopy data supported by HDM and provided textual feedback on the article, EAK performed the 3D STED experiments. HDM edited the article. CCH designed the experimental plan, supervised the research and edited the article.

### Conflict of interest

Casper Hoogenraad is an employee of Genentech, Inc., a member of the Roche group. The authors declare that they have no additional conflict of interest.

## References

- Ahmad FJ, Joshi HC, Centonze VE, Baas PW (1994) Inhibition of microtubule nucleation at the neuronal centrosome compromises axon growth. *Neuron* 12: 271–280
- de Anda FC, Pollarolo G, Da Silva JS, Camoletto PG, Feiguin F, Dotti CG (2005) Centrosome localization determines neuronal polarity. *Nature* 436: 704–708
- de Anda FC, Meletis K, Ge X, Rei D, Tsai LH (2010) Centrosome motility is essential for initial axon formation in the neocortex. *J Neurosci* 30: 10391–10406
- Andersen EF, Halloran MC (2012) Centrosome movements in vivo correlate with specific neurite formation downstream of LIM homeodomain transcription factor activity. *Development* 139: 3590–3599
- Baas PW, Deitch JS, Black MM, Banker GA (1988) Polarity orientation of microtubules in hippocampal neurons: uniformity in the axon and nonuniformity in the dendrite. *Proc Natl Acad Sci USA* 85: 8335–8339
- Barnes AP, Polleux F (2009) Establishment of axon-dendrite polarity in developing neurons. *Annu Rev Neurosci* 32: 347–381
- Basto R, Lau J, Vinogradova T, Gardiol A, Woods CG, Khodjakov A, Raff JW (2006) Flies without centrioles. *Cell* 125: 1375–1386
- van Beuningen SFB, Will L, Harterink M, Chazeau A, van Battum EY, Frias CP, Franker MAM, Katrukha EA, Stucchi R, Vocking K et al (2015) TRIM46 controls neuronal polarity and axon specification by driving the formation of parallel microtubule arrays. *Neuron* 88: 1208–1226
- van Beuningen SF, Hoogenraad CC (2016) Neuronal polarity: remodeling microtubule organization. *Curr Opin Neurobiol* 39: 1–7

- Castellanos E, Dominguez P, Gonzalez C (2008) Centrosome dysfunction in *Drosophila* neural stem cells causes tumors that are not due to genome instability. *Curr Biol* 18: 1209–1214
- Conduit PT, Wainman A, Raff JW (2015) Centrosome function and assembly in animal cells. *Nat Rev Mol Cell Biol* 16: 611–624
- Dent EW, Gupton SL, Gertler FB (2011) The growth cone cytoskeleton in axon outgrowth and guidance. *Cold Spring Harb Perspect Biol* 3: a001800
- Dotti CG, Sullivan CA, Banker GA (1988) The establishment of polarity by hippocampal neurons in culture. *J Neurosci* 8: 1454–1468
- Espuny-Camacho I, Michelsen KA, Gall D, Linaro D, Hasche A, Bonnefont J, Bali C, Orduz D, Bilheu A, Herpoel A et al (2013) Pyramidal neurons derived from human pluripotent stem cells integrate efficiently into mouse brain circuits in vivo. *Neuron* 77: 440–456
- Farina F, Gaillard J, Guerin C, Coute Y, Sillibourne J, Blanchoin L, Thery M (2016) The centrosome is an actin-organizing centre. *Nat Cell Biol* 18: 65–75
- Freal A, Rai D, Tas RP, Pan X, Katrukha EA, van de Willige D, Stucchi R, Aher A, Yang C, Altelaar AFM et al (2019) Feedback-driven assembly of the axon initial segment. *Neuron* 104: 305–321.e308
- Ishikawa H, Marshall WF (2011) Ciliogenesis: building the cell's antenna. *Nat Rev Mol Cell Biol* 12: 222–234
- Johnson MB, Sun X, Kodani A, Borges-Monroy R, Girsakis KM, Ryu SC, Wang PP, Patel K, Gonzalez DM, Woo YM et al (2018) Aspm knockout ferret reveals an evolutionary mechanism governing cerebral cortical size. *Nature* 556: 370–375
- Kole MH, Ilschner SU, Kampa BM, Williams SR, Ruben PC, Stuart GJ (2008) Action potential generation requires a high sodium channel density in the axon initial segment. *Nat Neurosci* 11: 178–186
- Kuijpers M, van de Willige D, Freal A, Chazeau A, Franker MA, Hofenk J, Rodrigues RJ, Kapitein LC, Akhmanova A, Jaarsma D et al (2016) Dynein regulator NDEL1 controls polarized cargo transport at the axon initial segment. *Neuron* 89: 461–471
- Lancaster MA, Renner M, Martin CA, Wenzel D, Bicknell LS, Hurler ME, Homfray T, Penninger JM, Jackson AP, Knoblich JA (2013) Cerebral organoids model human brain development and microcephaly. *Nature* 501: 373–379
- Leterrier C (2018) The axon initial segment: an updated viewpoint. *J Neurosci* 38: 2135–2145
- Linaro D, Vermaercke B, Iwata R, Ramaswamy A, Libe-Philippot B, Boubakar L, Davis BA, Wierda K, Davie K, Poovathingal S et al (2019) Xenotransplanted human cortical neurons reveal species-specific development and functional integration into mouse visual circuits. *Neuron* 104: 972–986.e976
- Lindhout FW, Cao Y, Kevenaar JT, Bodzeta A, Stucchi R, Boumpoutsari MM, Katrukha EA, Altelaar M, MacGillavry HD, Hoogenraad CC (2019) VAP-SCRN1 interaction regulates dynamic endoplasmic reticulum remodeling and presynaptic function. *EMBO J* 38: e101345
- Lindhout FW, Kooistra R, Portegies S, Herstel LJ, Stucchi R, Snoek BL, Altelaar AM, MacGillavry HD, Wierenga CJ, Hoogenraad CC (2020) Quantitative mapping of transcriptome and proteome dynamics during polarization of human iPSC-derived neurons. *eLife* 9: e58124
- Lois C, Hong EJ, Pease S, Brown EJ, Baltimore D (2002) Germline transmission and tissue-specific expression of transgenes delivered by lentiviral vectors. *Science* 295: 868–872
- Martin M, Veloso A, Wu J, Katrukha EA, Akhmanova A (2018) Control of endothelial cell polarity and sprouting angiogenesis by non-centrosomal microtubules. *eLife* 7: e33864
- Meka DP, Scharrenberg R, Zhao B, Kobler O, König T, Schaefer I, Schwanke B, Klykov S, Richter M, Eggert D et al (2019) Radial somatic F-actin organization affects growth cone dynamics during early neuronal development. *EMBO Rep* 20: e47743
- Meka DP, Scharrenberg R, Calderon de Anda F (2020) Emerging roles of the centrosome in neuronal development. *Cytoskeleton* 77: 84–96
- Mennella V, Keszthelyi B, McDonald KL, Chhun B, Kan F, Rogers GC, Huang B, Agard DA (2012) Subdiffraction-resolution fluorescence microscopy reveals a domain of the centrosome critical for pericentriolar material organization. *Nat Cell Biol* 14: 1159–1168
- Moritz M, Braunfeld MB, Guenebaut V, Heuser J, Agard DA (2000) Structure of the gamma-tubulin ring complex: a template for microtubule nucleation. *Nat Cell Biol* 2: 365–370
- Nakazawa Y, Hiraki M, Kamiya R, Hirono M (2007) SAS-6 is a cartwheel protein that establishes the 9-fold symmetry of the centriole. *Curr Biol* 17: 2169–2174
- Nano M, Basto R (2017) Consequences of centrosome dysfunction during brain development. *Adv Exp Med Biol* 1002: 19–45
- Otani T, Marchetto MC, Gage FH, Simons BD, Livesey FJ (2016) 2D and 3D stem cell models of primate cortical development identify species-specific differences in progenitor behavior contributing to brain size. *Cell Stem Cell* 18: 467–480
- Pasantes-Morales H (1996) Volume regulation in brain cells: cellular and molecular mechanisms. *Metab Brain Dis* 11: 187–204
- Perez-Riverol Y, Csordas A, Bai J, Bernal-Llinares M, Hewapathirana S, Kundu DJ, Inuganti A, Griss J, Mayer G, Eisenacher M et al (2019) The PRIDE database and related tools and resources in 2019: improving support for quantification data. *Nucleic Acids Res* 47: D442–D450
- Pulvers JN, Bryk J, Fish JL, Wilsch-Brauninger M, Arai Y, Schreier D, Naumann R, Helppi J, Habermann B, Vogt J et al (2010) Mutations in mouse Aspm (abnormal spindle-like microcephaly associated) cause not only microcephaly but also major defects in the germline. *Proc Natl Acad Sci USA* 107: 16595–16600
- Shalem O, Sanjana NE, Hartenian E, Shi X, Scott DA, Mikkelsen T, Heckl D, Ebert BL, Root DE, Doench JG et al (2014) Genome-scale CRISPR-Cas9 knockout screening in human cells. *Science* 343: 84–87
- Shi Y, Kirwan P, Livesey FJ (2012) Directed differentiation of human pluripotent stem cells to cerebral cortex neurons and neural networks. *Nat Protoc* 7: 1836–1846
- Sousa AMM, Meyer KA, Santpere G, Gulden FO, Sestan N (2017) Evolution of the human nervous system function, structure, and development. *Cell* 170: 226–247
- Stiess M, Maghelli N, Kapitein LC, Gomis-Ruth S, Wilsch-Brauninger M, Hoogenraad CC, Tolic-Norrelykke IM, Bradke F (2010) Axon extension occurs independently of centrosomal microtubule nucleation. *Science* 327: 704–707
- Stoeckli ET (2018) Understanding axon guidance: are we nearly there yet? *Development* 145: dev151415
- Tsai LH, Gleeson JG (2005) Nucleokinesis in neuronal migration. *Neuron* 46: 383–388
- van der Vaart B, van Riel WE, Doodhi H, Kevenaar JT, Katrukha EA, Gumy L, Bouchet BP, Grigoriev I, Spangler SA, Yu KL et al (2013) CFEOM1-associated kinesin KIF21A is a cortical microtubule growth inhibitor. *Dev Cell* 27: 145–160
- Vora SM, Phillips BT (2016) The benefits of local depletion: the centrosome as a scaffold for ubiquitin-proteasome-mediated degradation. *Cell Cycle* 15: 2124–2134
- Willems J, de Jong APH, Scheefhals N, Mertens E, Catsburg LAE, Poorthuis RB, de Winter F, Verhaagen J, Meje FJ, MacGillavry HD (2020) ORANGE: a CRISPR/Cas9-based genome editing toolbox for epitope tagging of endogenous proteins in neurons. *PLoS Biol* 18: e3000665



- Witte H, Neukirchen D, Bradke F (2008) Microtubule stabilization specifies initial neuronal polarization. *J Cell Biol* 180: 619–632
- Wong YL, Anzola JV, Davis RL, Yoon M, Motamedi A, Kroll A, Seo CP, Hsia JE, Kim SK, Mitchell JW et al (2015) Cell biology. Reversible centriole depletion with an inhibitor of Polo-like kinase 4. *Science* 348: 1155–1160
- Yau KW, van Beuningen SF, Cunha-Ferreira I, Cloin BM, van Battum EY, Will L, Schatzle P, Tas RP, van Krugten J, Katrukha EA et al (2014) Microtubule minus-end binding protein CAMSAP2 controls axon specification and dendrite development. *Neuron* 82: 1058–1073
- Yau KW, Schatzle P, Tortosa E, Pages S, Holtmaat A, Kapitein LC, Hoogenraad CC (2016) Dendrites in vitro and in vivo contain microtubules of opposite polarity and axon formation correlates with uniform plus-end-out microtubule orientation. *J Neurosci* 36: 1071–1085
- Zhao B, Meka DP, Scharrenberg R, König T, Schwanke B, Kobler O, Windhorst S, Kreutz MR, Mikhaylova M, Calderon de Anda F (2017) Microtubules modulate F-actin dynamics during neuronal polarization. *Sci Rep* 7: 9583
- Zmuda JF, Rivas RJ (1998) The Golgi apparatus and the centrosome are localized to the sites of newly emerging axons in cerebellar granule neurons in vitro. *Cell Motil Cytoskelet* 41: 18–38



**License:** This is an open access article under the terms of the Creative Commons Attribution-NonCommercial-NoDerivs License, which permits use and distribution in any medium, provided the original work is properly cited, the use is non-commercial and no modifications or adaptations are made.